Dynamic Analysis and Parametric Optimization of Telescopic Tubular Mast Applied on Solar Sail

Chen-Yang Ji
Shenyang Institute of Automation Chinese Academy of Sciences https://orcid.org/0000-0002-8866-1465

Jin-Guo Liu (liujinguo@sia.cn)
Shenyang Institute of Automation, Chinese Academy of Science

Chen-Chen Wu
Shenyang Institute of Automation Chinese Academy of Sciences

Peng-Yuan Zhao
Shenyang Institute of Automation Chinese Academy of Sciences

Ke-Li Chen
Shenyang Institute of Automation Chinese Academy of Sciences

Original Article

Keywords: Telescopic tubular mast, Solar sail, Genetic algorithm, Modal analysis, optimization

Posted Date: December 1st, 2020

DOI: https://doi.org/10.21203/rs.3.rs-116065/v1

Title page

Dynamic analysis and parametric optimization of telescopic tubular mast applied on solar sail

Chen-Yang Ji, born in 1994, is currently a master candidate at *Northeastern University and State Key Laboratory of Robotics, Shenyang Institute of Automation, Chinese Academy of Science, China.*
E-mail: jichenyang@sia.cn

Jin-Guo Liu, born in 1978, is currently a professor and a PhD candidate supervisor at *Shenyang Institute of Automation, Chinese Academy of Science, China.*
E-mail: liujinguo@sia.cn

Chen-Chen Wu, born in 1990, is currently an associate professor at *Shenyang Institute of Automation, Chinese Academy of Science, China*.
E-mail: wuchenchen@sia.cn

Peng-Yuan Zhao, born in 1994, is currently a PhD candidate at *State Key Laboratory of Robotics, Shenyang Institute of Automation, Chinese Academy of Science, China.*
E-mail: zhaopengyuan@sia.cn

Ke-Li Chen, born in 1991, is currently an engineer at *Shenyang Institute of Automation,Chinese Academy of Science, China*.
E-mail: chenkeli@sia.cn

Corresponding author：Jin-Guo Liu　E-mail：liujinguo@sia.cn

ORIGINAL ARTICLE

Dynamic analysis and parametric optimization of telescopic tubular mast applied on solar sail

Chen-Yang Ji[1, 2, 3] • Jin-Guo Liu[1, 3,*] • Chen-Chen Wu[1, 3] • Peng-Yuan Zhao[1, 3, 4] • Ke-Li Chen[1, 3]

*

Abstract: The Telescopic Tubular Mast (TTM) has excellent performance and is widely used in aerospace. Reasonable parameter design and optimization can shorten development cycle and improve performance for TTM. This paper designed a TTM driven by the bistable carbon reeled composite boom. The equivalent model of the TTM is established and simulated, which can be used as ex-tending structure for the solar sail. The work flow of the solar sail with the TTM is introduced. The natural frequency of the equivalent model and the segmented model is solved respectively using ABAQUS. The TTM under six different load conditions is analyzed. The influence of different factors on the vibration characteristics of the TTM is analyzed and the sensitivity analysis is carried out. Parameters including stiffness, natural frequency, mass and extension ratio are optimized using the multi-objective genetic optimization algorithm. According to the optimization results, the prototype was processed, and the experiment was completed with the equivalent load of solar sail. It provides a reference for the parametric design of the TTM.

Keywords: Telescopic tubular mast • Solar sail • Genetic algorithm • Modal analysis • optimization

1 Introduction

As an important part of the spacecraft, the TTM has been studied extensively scholars around the world. With the development of space technology, the space extension mechanism is developing towards large-diameter, high-precision, and lightweight. Furthermore, it has high requirements for the extension ratio, strength and stability.

The space deployable structures represent frontier of the extension mechanism, which is applied in various fields. In the field of interstellar voyages, the extension arm can be used as a support structure for large solar sails. The extension arm is used to keep the solar sail at a certain distance from the spacecraft and perform extension work. There are many types of space deployable structures, mainly including hinged truss extension arms, thin-walled tubular extension arms, inflatable extension arms, and tension integration system extension arms [1-3]. Especially, the thin-walled tubular extension arm has been a research hotspot of space deployment mechanism due to its advantages in weight and deployment reliability. Many researchers have also carried out related research on thin-walled tubular extension arms, including structural parameter optimization, environmental coupling analysis, material blossoming, etc. Yildiz et al. used particle swarm intelligence algorithm to optimize the size and prestress of the extension arm of the tension structure [4]. Yang et al. optimized the stretching and winding process of the c-section thin-walled composite stretch arm, and obtained the best design parameters of the stretch arm by using the NLPQL algorithm [5]. Bai et al conducted thermal and winding analysis of the lenticular composite extension arm in a simulated space environment. The results show that the temperature difference between the radiated surface and the shadow surface will cause large deformation [6-7]. Jordan conducted experiments on the traction device of the lenticular extension arm, which realized the extension and contraction of the lenticular ex-tension arm and prevented blossoming [8]. Ding et al. de-signed and analyzed the winding device of the rope-driven space deployable structures [9]. Soykasap et al. conducted research on composite hinges and ribbon springs used to extension arms [10-13]. Different extension arms have their own advantages and disadvantages. The stability and high strength of the extension arms are the key to the successful completion of the mission during interstellar voyages.

* Correspondence: liujinguo@sia.cn
[1]State Key Laboratory of Robotics, Shenyang Institute of Automation, Chinese Academy of Science, 110016, China

Among them, the space extension arm can be used as the support structure of the solar sail due to its advantages of high precision, high strength, high reliability, etc. Therefore, it is necessary to analyze its dynamic characteristics and carry out parameterized design and optimization.

The TTM was first applied to the Dornier system in Ger-many, and its deployment length can reach 25m, which is used as a military communication facility. The American NRTHROB GRUMMAN company and the German Dornier company are in a leading position in the field of TTM, and have relatively mature research and applications. The thrust per unit area is relatively small, so the solar sails used for interstellar sailing missions generally have a large size to obtain sufficient thrust. Joachim et al have developed a lenticular ultra-light extendable arm that can be used in space missions such as solar sails, and conducted zero-gravity experiments [14]. Michael designed a windable truss mast for solar sails, which can reach 100-1000m in length [15]. Christoph et al. designed and experimented with the Carbon Fibre Reinforced Plastic extension arm used on the solar sail and proposed improvements to prepare for future missions [16-17]. Johnson et al summarized and prospected NASA's research on solar sails [18]. In addition to the application on solar sails, the TTM can also be ap-plied to the extension mechanism of off-orbit sails. Craig and his colleagues used inflatable masts to support off-orbit sails to successfully complete the off-orbit mission, and the satellite re-entered the atmosphere after 72 days [19]. Juan et al designed and developed the off-orbit sails for low earth orbit, and carried out full-scale deployment and impact tests [20]. Wei et al. studied and analyzed the inflatable arms and membrane folds of the inflatable deployable so-lar sail [21]. Mark et al have also conducted related re-search on inflatable extension arms [22-24].

This paper aims to proceed dynamic analysis and para-metric optimization for the TTM structure we designed. The stretching unit and driving structure of the TTM is designed in Section 2. The Euler-Bernoulli continuous beam theory is used to establish the dynamic model of the TTM in Section 3. In addition, the convergence of the Euler-Bernoulli beam and the segmental model of TTM for the equivalent model is analyzed and the modal analysis results are compared using ABAQUS. The vibration characteristics with different working conditions are analyzed in Section 4. Six factors including material, diameter, wall thickness, and number of sections is selected to analyze their influence for the vibration characteristics, and then sensitivity analysis is per-formed. In Section 5, the multi-objective genetic algorithm is used to optimize the natural frequency, mass, bending rigidity, and extension ratio of the TTM. The deployment experiments with tip-load are carried out in Section 6 and the conclusion is summarized in Section 7.

2 Structure design of TTM

The TTM is mainly composed of two parts: stretching unit and driving structure. Its main structure is shown in Figure 1, mainly including bistable carbon fiber, motor, reel, stretching unit, roller, etc. The motor is fixed by a flange and drives the reel. The bistable carbon fiber is stretched out under the drive of the motor. The roller prevents the carbon fiber from blossoming, and the reel is used to store the bistable carbon fiber. The stretching unit is extended step by step under the action of the driving structure to complete the deployment. The stretching unit is composed of thin-walled tube with the same length, and the wall thickness is generally thin in order to reduce the mass. The tube relies on the internal pin to complete the locking, which improves the rigidity and load capacity. The outer arm of the tube is provided with a guide groove, and the guide rail is matched with the groove to avoid circumferential rotation and damage to the internal structure.

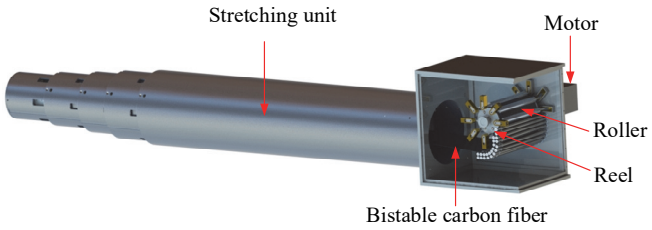

Figure 1 The main structure of each part of the TTM

The power to extend the tube is provided by the drive mechanism. The motor drives the reel to extend the bistable carbon fiber, and the top of the bistable carbon fiber is connected to the tube. As shown in Figure 2, in order to avoid blossoming of the carbon fiber, multiple rollers are used to compress the bistable carbon fiber circumferentially. The two ends of the circumferentially distributed roller are placed in the bearings inside the slider, so that it can roll smoothly and reduce the friction with the carbon fiber. The bottom end of the slider can accommodate a compression spring of a certain length, and the other end of the com-pression spring is in contact with the side wall. It should be noted that the length of the

compression spring should be slightly larger to ensure that the bistable carbon fiber on the reel can still provide enough radial force to prevent blossoming, as shown in the Figure 2.

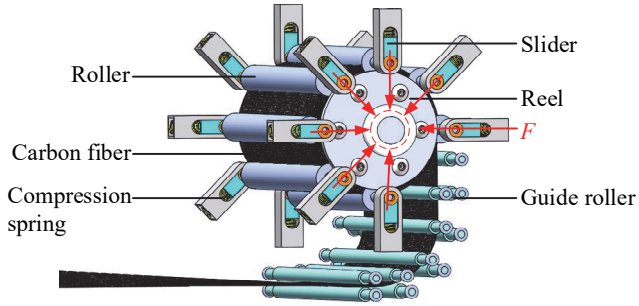

Figure 2 Drive and anti-blossoming structure

Compared with the traditional space deployable structures, the use of a new structure and the use of bistable carbon fiber will greatly reduce the weight of the TTM, re-duce the complexity of the structure, and greatly increase the success rate of space missions. In addition, the use of carbon fiber in the tube can not only reduce the weight, but the advantages of carbon fiber itself, such as corrosion resistance and high strength, are also conducive to the execution of aviation tasks.

3 Dynamic analysis of TTM

The additional load at the top of the TTM is solar sail. As shown in Figure 3, the solar sail can provide power for spacecraft that perform interstellar missions, save fuel, re-duce launch load, and carry more equipment. Solar sails rely on pressure to obtain thrust.

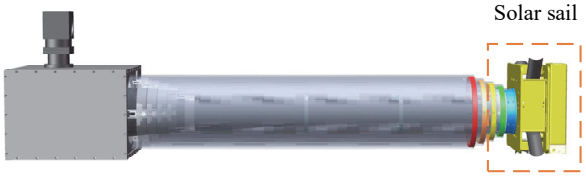

Figure 3 Solar Sail Load at the tip of TTM

The solar sail is placed on the top of the TTM and reaches the designated orbit for deployment. The TTM keeps the solar sail away from the spacecraft to prevent the sail membrane from affecting the spacecraft or causing damage to the sail membrane in contact with the space-craft. The working process is shown in Figure 4. The TTM is deployed step by step under the drive of the motor. When the TTM is deployed to the maximum length, the top solar sail starts to work until it is fully deployed.

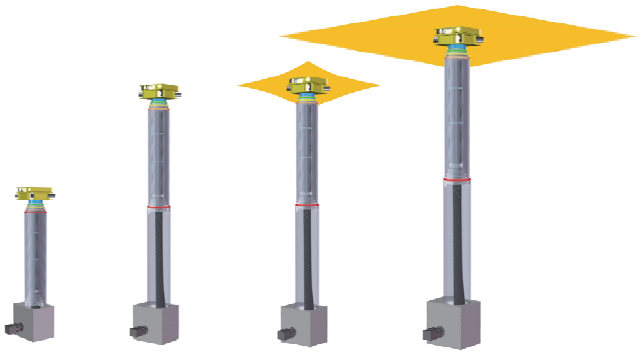

Figure 4 Work flow of TTM and solar sail

There are many complicated parts in the TTM. In addi-tion to the tube and the mounting ring, it also includes some smaller parts, such as pins and springs. If the model can be simplified in the finite element simulation analysis, it can greatly reduce the workload in the analysis process, im-prove efficiency and save computing resources. After the TTM is deployed, it can be regarded as a continuum struc-ture with uniform mass distribution, which satisfies the as-sumption of perfect elastic body and the assumption of small deformation. The equivalent beam micro-element section is shown in Figure 5.

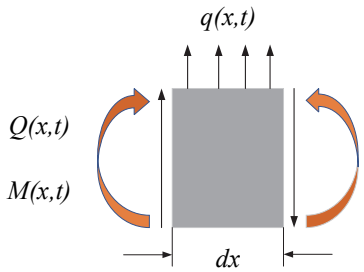

Figure 5 Equivalent beam micro-element segment model

Using the D'ALEMBERT principle, the lateral force bal-ance equation of the equivalent beam micro-element sec-tion can be obtained as show in Equation (1).

$$Q(x,t)+q(x,t)dx-\left(Q(x,t)+\frac{\partial Q}{\partial x}dx\right)-\rho A(x)\frac{\partial^2 y}{\partial t^2}dx=0 \qquad (1)$$

After Equation (1) is sorted, the Equation(2) can be ob-tained.

$$M+\frac{\partial M}{\partial x}dx-M-Qdx-\left[q(x,t)dx-\rho A(x)\frac{\partial^2 y}{\partial t^2}dx\right]\frac{dx}{2}=0 \qquad (2)$$

Bring in the relevant parameters and finally get the Equation (3).

$$f_1 = \frac{1.875^2}{2\pi}\sqrt{\frac{ED^4(1-\alpha^4)}{64\rho(D^2-d^2)l^4}} \quad (3)$$

Where q is the uniform load, Q is the shear force, M is the bending moment, D is the outer diameter, d is the inner diameter, l is the length, and α is the ratio of the inner diameter to the outer diameter.

3.1 TTM equivalent model

Establish the contraction state model and the extension equivalent model respectively, as shown in Figure 6.

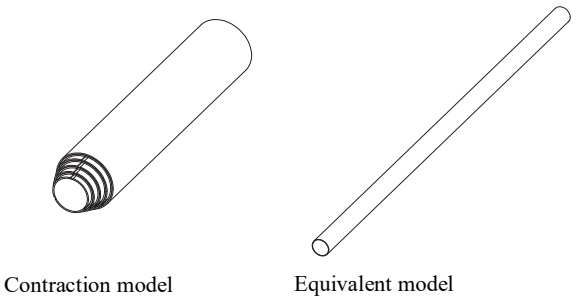

Figure 6 Model of TTM contraction and extension state

The finite element model is established by ABAQUS. The model needs to be meshed before the analysis. The size of the mesh has a great influence on the accuracy of the analysis results. When the mesh size is too large, the analy-sis result error will exceed the allowable value. Too small a size will lead to long calculation time, waste of calculation resources and limited accuracy improvement. Therefore, mesh convergence analysis is required before meshing. Un-der the premise of ensuring accuracy, the calculation time is shortened as much as possible to save calculation re-sources.

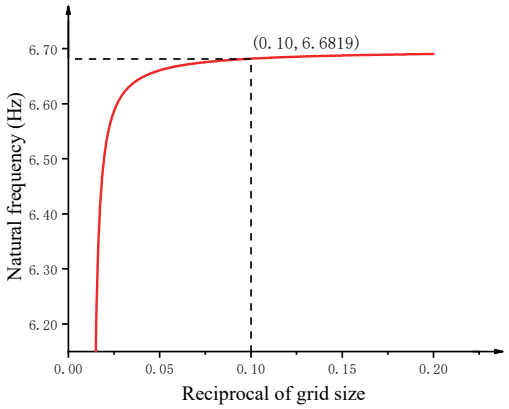

Figure 7 Mesh size convergence analysis

Convergence analysis on the mesh size, the results are shown in Figure 7. It can be seen from the figure that the curve tends to be stable after the abscissa 0.1, so the model can be meshed with a 10mm grid on the premise of saving computing resources.

3.2 Equivalent model verification and modal analysis

After the equivalent model is established, first verify the consistency of the analysis results of the segmented model and the equivalent model to ensure the accuracy of the subsequent analysis. The segmented model and equivalent model of the TTM are established respectively, and the grid size provided in the previous section is divided into grids. TTM uses 7075-aluminum alloy for finite element analysis to verify the accuracy of the equivalent model.

The modal shape and vibration frequency of the two models are analyzed, and the modal shape is shown in the Figures 8 and 9.

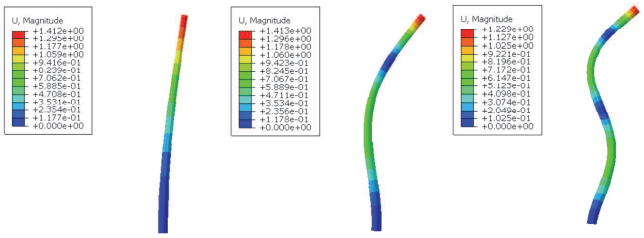

Figure 8 Modal shape of the segmented model of the TTM

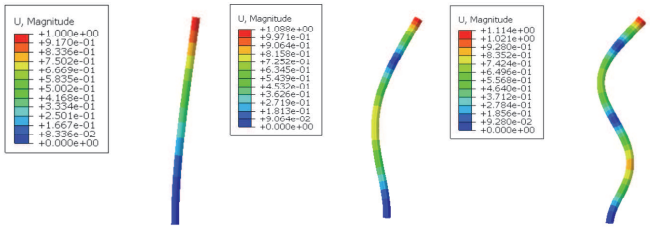

Figure 9 Modal shape of the equivalent model of the TTM

It can be seen that the equivalent model and the seg-mented model have the same mode shape. The frequencies of each order are shown in Table 1. The frequency of each order of the segmented model and the equivalent model is close to the calculation result of the dynamic equation. The frequency of 6.68Hz has good consistency, so the equiva-lent model can be used to analyze the influence of various factors on vibration characteristics.

Table 1 Frequency of each step of the TTM/Hz

Model	1	3	5	7
Segmented model	8.92	43.15	109.46	194.27
Equivalent model	6.68	41.26	113.32	147.21

4 Influence of different factors on vibration characteristics

4.1 Different fixing methods and loads

There are many factors that affect the vibration characteristics of the TTM. During the transportation phase, the ex-tension arm is in a contraction state, and its fixing method and load will affect its vibration characteristics. In addition, the material, diameter, and wall thickness of the TTM also affect its own vibration characteristics, so this section will analyze from two aspects separately.

Table 2 The parameters of the solar sail

length/mm	width/mm	high/mm	weight/kg	Expanded area/m^2
100	100	49.3	1.1	0.53

There are two ways to fix the TTM during transportation, which are fixed at the bottom end or fixed at both ends. In the extension state, it can also be divided into two situations according to the load. Different fixing methods have a certain influence on the rigidity of the structure. Establish analysis models according to different fixing methods, and extract and analyze the natural frequency. In addition, when the solar sail is fixed on the top as a load, it will affect the vibration characteristics of the TTM There are 6 situations to be analyzed for the TTM, as shown in Table 3.

Table 3 Different states and loads of TTM

condition	A	B	C	D	E	F
Expanded state	—	—	—	—	Yes	Yes
Collapsed state	Yes	Yes	Yes	Yes	—	—
Top fixed	—	—	Yes	Yes	—	—
Bottom fixed	Yes	Yes	Yes	Yes	Yes	Yes
Load	—	Yes	—	Yes	—	Yes

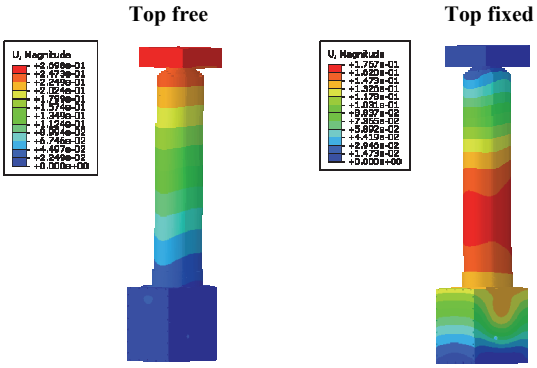

Figure 10 Displacement cloud diagram under two conditions

Figure 10 is the displacement cloud diagram of two conditions when the equivalent load of solar sail is installed on the top of the extension arm in the contraction state.

Analyzing the above six situations, the base of the ex-tension arm is connected with the platform by bolts to keep it stable during transportation. In addition, the model needs to be simplified before the analysis. In order to avoid the appearance of poor quality meshes, unnecessary small chamfers must be removed. The analysis data of the six situations are sorted out, and the results are shown in Table 4.

Table 4 Comparison of the first six-order frequencies in six situations (Hz)

Mode	A	B	C	D	E	F
1	66.55	64.31	307.71	306.00	6.67	6.38
2	76.59	74.04	322.57	320.80	6.67	6.38
3	361.58	353.14	420.05	430.06	41.26	39.50
4	370.78	363.49	430.48	430.48	41.26	39.50
5	426.74	426.41	441.88	441.83	113.32	108.61
6	429.91	430.45	509.47	509.38	113.32	108.61

It can be seen from Table 4 that the natural frequency difference between A and C is relatively large, and the highest increase reached 362.35%. The difference in the fixed method has brought a larger natural frequency increase. The simulation results of the six working conditions of the TTM show that the load has a certain influence on the natural frequency. Due to its small size and light weight, the rigidity of the overall structure does not change much, and there is a slight decrease in natural frequency. According to the comprehensive analysis results, it is advisable to adopt the method of fixing at both ends for transportation, which is beneficial to avoid lower frequency vibration and prevent structural damage caused by resonance.

4.2 Influence of other factors

In addition to the above-mentioned effects of the fixing method and load of the extension arm, its vibration characteristics are mainly related to its own properties. This section explored the impact on the vibration characteristics of the TTM from 4 aspects, namely material, wall thickness, diameter, Section number. First, analyze the influence of the material on the modal of the TTM, and the material analysis can provide support for the subsequent design of the product. The specific parameters of commonly used aero-space materials used in this section are shown in Table 5.

Table 5 Material characteristic parameters

Material	E/Gpa	ν	ρ/kg·m^{-3}	Thickness/mm	Length/mm
Al-7075	72	0.33	2.8×10^{3}	5	5320
T700	60	0.3	1.6×10^{3}	5	5320
Mg alloy	42.2	0.28	1.76×10^{3}	5	5320
45#	193	0.3	7×10^{3}	5	5320

By assigning different materials to the model, the frequency information under different materials of the TTM is obtained. The frequencies under the corresponding orders of the four materials are plotted as follows. It can be seen from the figure 11 that the frequency of the extension arm made of carbon fiber T700 is significantly improved com-pared with other materials, and its natural frequency (first-order frequency) is increased by about 16.6%~25.1%. Therefore, carbon fiber materials should be preferred in the design of the extension arm. Although the 45 steel is better than 7075 aluminum alloy in natural frequency, its high density increases the transportation cost. To a certain extent, magnesium alloy can replace aluminum alloy due to its lower density and excellent vibration characteristics. Through the comparison and analysis of the results, the overall performance of carbon fiber is the best, followed by aluminum alloy, magnesium alloy and 45# steel.

The wall thickness of the TTM not only affects its overall weight, but also has a greater impact on the vibration characteristics. In this paper, the wall thickness is used as a variable to design, and the material is T700 carbon fiber, with a 0.5mm gradient, to study the vibration characteristics of an extension arm with a thickness of 1-5mm.

Figure 12 is drawn according to the data obtained by the simulation. It can be seen that as the wall thickness gradually increases, the frequencies of each order including the natural frequency gradually increase. When the wall thick-ness is 5mm, the high-order frequency increases greatly. Its natural frequency is 2.84% higher than that of 1mm wall thickness. The relationship between weight and frequency should be considered when designing the extension arm, and a smaller wall thickness should be selected on the premise of meeting the frequency requirements.

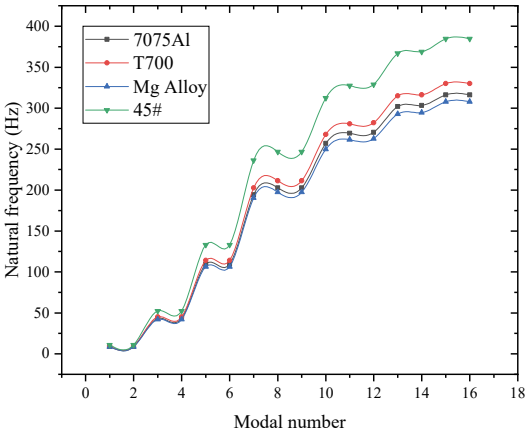

Figure 11 The influence of material on vibration characteristics

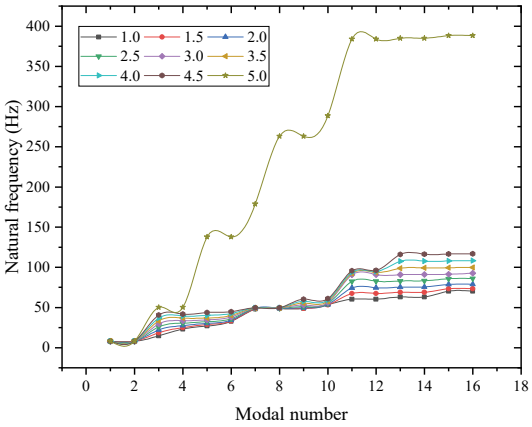

Figure 12 The influence of wall thickness on vibration characteristics

Due to the limitation of carrying space, the storage volume of TTM should be as small as possible. The diameter of the TTM tube has a direct effect on the volume, so it is necessary to study the influence of different diameters on the vibration characteristics. With a diameter of 180mm as the benchmark, the influence of the diameter on its vibration characteristics is studied with an increment of 10mm. It can be seen from Figure 13 that when the wall thickness and length are constant, the natural frequency increases slightly with the increase of

the diameter, while the higher-order frequency decreases. The diameter is selected according to the analysis results. The small diameter should be selected when the natural frequency does not change much. In addition, the small diameter helps to increase high-order frequencies and reduce weight.

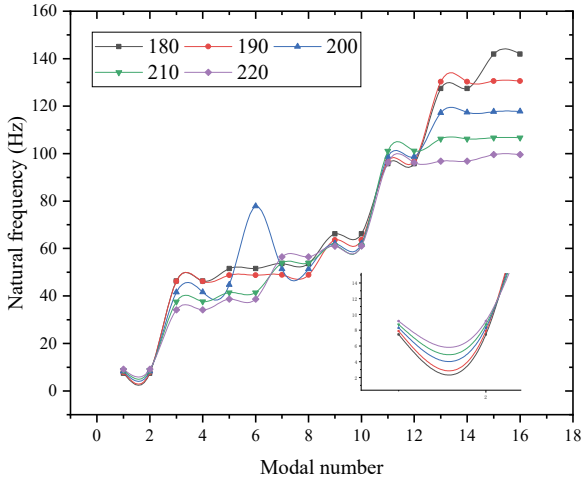

Figure 13 The influence of diameter on vibration characteristics

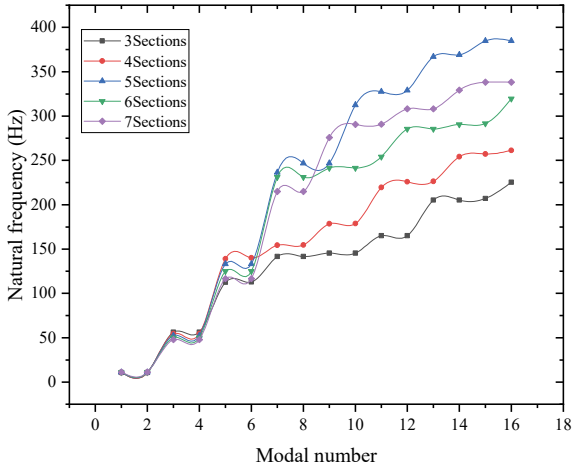

Figure 14 The influence of number of sections on vibration characteristics

Extension ratio is an important performance index of space extension structure. The number of sections has a direct effect on the extension ratio of the TTM. The volume of the launch vehicle is limited, and the large extension ratio means a smaller storage length, making full use of the carrying space. When the length is constant, the increase of sections will bring about a greater extension ratio, but the number of sections should also be limited to a certain range to obtain better performance. In this section, the length and material of the TTM remain unchanged, and the number of sections is selected from 3 to 7 in order to study the influence of the number of sections on its vibration. When the number of sections is 5, its natural frequency is 2.81% higher than that of 3 sections, and 3.42% lower than that of 7 sections. The result of the extension ratio is shown in Figure 14. It can be seen that as the number of sections in-creases, the natural frequency increases slightly. When the natural frequency does not change much, the number of sections should be selected as much as possible to obtain a larger extension ratio and excellent vibration characteristics.

4.3 Sensitivity analysis

In order to study the of influence of different factors on the vibration characteristics, the sensitivity analysis was carried out using the method of operations research to analyze the influence of different factors on the TTM. The sensitivity analysis equation is as follows:

$$\eta\left(f_i / x_j\right)=\lim_{\Delta x_j \to 0} \frac{\left(\Delta f_i / f_i\right)}{\left(\Delta x_j / x_j\right)} \tag{4}$$

Among them, f_i and x_j are not 0, Δf_i and Δx_j are natural frequency variations and parameter variations, x_j and f_i are structural parameters and natural frequencies under corresponding parameters. The sensitivity chart is drawn based on the simulation analysis result as in Table 6.

Table 6 Sensitivity analysis under different factors

$i=j$	1	2	3	4	average value
Wall thickness	0.0054	0.0054	0.0054	0.0117	0.0070
diameter	1.0206	1.0223	1.0206	1.0189	1.0206
Section number	0.0068	0.1219	0.0566	0.1361	0.3080

It can be seen from the sensitivity analysis table that the value has positive and negative values. Positive value means an increase in the natural frequency, and negative value is the opposite. It can be seen that the influence of the change of diameter on the vibration characteristics is greater than the influence of the number of sections and the wall thickness. The influence of the diameter on the vibration characteristics should be given priority in the design. When the natural frequency needs to meet the task requirements, the diameter should be given priority.

5 Multi-objective genetic algorithm optimization

In the design of the TTM, the allowable space and weight

are generally given according to the transportation conditions, and then the parameterized design is carried out. Kalyanmoy Deb et al. proposed a genetic algorithm based on non-dominated sorting, which has excellent solution performance [25].

In this section, the multi-objective intelligent algorithm is used to optimize within the given parameter range. There are many multi-objective intelligent optimization algorithms, but the most widely used is the non-dominated sorting genetic algorithm with elite strategy (NASG-II). Genetic algorithm is an evolutionary algorithm designed based on the principle of 'natural selection, survival of the fittest' in nature. The improved genetic algorithm in MATLAB is used to optimize the multi-objectives.

5.1 Objective function and feasible range

The design of the TTM needs to optimize the parameters of multiple objective functions. Multi-objective optimization can be understood as the minimum or maximum value of multiple objective functions under constraints. In general, the optimal solution of the multi-objective function is not unique, there is a game between variables, and the result is the Pareto optimal front.

The mathematical model of multi-objective function can be expressed as equation (5).

$$\begin{cases} \min/\max y = (f_1(x), \cdots, f_n(x)) \\ x = (x_1, \cdots, x_n) \end{cases} \tag{5}$$

Where f is the objective function, x is the variable, and n is the number of variables.

Variables need to be optimized within a given feasible region. If the feasible region is not specified, the amount of calculation will be large and the parameters obtained do not meet actual requirements. Therefore, it is necessary to assign parameter ranges to the variables and obtain the optimal solution of the objective function for selection.

After completing the design of the TTM, the feasible region of the objective function is specified, and then the optimization work is carried out. The TTM is installed inside the transport rocket, and its height, radius, weight, etc. need to be designed according to actual conditions. The extension and contraction length of the TTM determine its extension ratio. The extension ratio should be as large as possible to reduce storage space. The diameter should be reasonably selected according to the overall length and working properties while ensuring sufficient strength and meeting the storage space.

The objective functions to be optimized are shown in Equation (6).

Where E is the elastic modulus of the material, ρ is the material density, I is the section moment of inertia, and α is the radius ratio.

$$\min f(x)\begin{cases} f(1) = \dfrac{1.875^2}{2\pi}\sqrt{\dfrac{EI}{\rho A l^4}} \\ f(2)=\pi\left(\left(\dfrac{D}{2}\right)^2-\left(\dfrac{d}{2}\right)^2\right)l\rho \\ f(3)=E\dfrac{\pi D^4\left(1-\alpha^4\right)}{64} \\ f(4)=\left(l/x_4\right)/l \end{cases} \tag{6}$$

Because the matrix operation is used in the optimization process, the independent variable is the column vector of $\boldsymbol{x}$, and the variable is replaced with the sequence of $\boldsymbol{x}$ when writing the program. The objective function is the minimum value in the optimization process. Therefore, if we want to obtain the maximum value of the function, we should take the reciprocal of it as the objective function. The feasible range of parameters is shown in Table 7.

Table 7 Parameter feasible region

Variable	Feasible region
Outer diameter（*x1*）	0.15~0.20m
Wall thickness（*x2*）	0.002~0.005m
length（*x3*）	4.8~5.2m
Section number（*x4*）	5~10m

5.2 Parameter optimization

When the objective function and feasible region are given, the optimization of the objective function can be carried out. Compared with traditional optimization algorithms, the random characteristics of genetic algorithms can avoid falling into local optimum and find the global optimum. Traditional algorithms are generally used to solve structured problems with clear constraints. They generally have the only best advantage and are not suitable for multi-extreme problems. For the four objective functions in this paper, there are multiple optimal solutions in the feasible range, so the multi-objective genetic algorithm can quickly obtain the optimal solution set of the variables.

Set the parameters of the multi-objective genetic algorithm, including the optimal front-end individual coefficient, population size, evolutionary algebra, etc. The

related parameters are shown in Table 8.

Table 8 Genetic algorithm parameter settings

Parameter	Value
ParetoFraction	0.3
PopulationSize	200
MaxGeneration	300
stallGenLimit	300
TolFun	$1e^{-10}$
Crossover ratio	0.8
Mutation ratio	0.2

After setting the parameters, the Gamultiobj function is used to solve the problem based on the equivalent model of the TTM, and the Pareto solution set of the multi-objective function is obtained. The results are shown in Table 9, where D is the diameter, T is the wall thickness, L is the length, N is the number of sections, F is the natural frequency, M is the mass, K is the bending rigidity, and W is the extension ratio.

Table 9 Multi-objective optimization Pareto solution set

D/mm	T/mm	L/m	N	F/Hz	M/Kg	K/N·m^2	W
150.00	2.00	4.80	9.99	6.43	12.54	1.8E+05	0.10
199.97	2.33	4.81	9.55	8.56	19.51	5.1E+05	0.10
199.95	4.98	5.07	9.71	7.60	43.46	1.0E+06	0.10
199.97	2.08	4.81	9.77	8.57	17.48	4.6E+05	0.10
199.87	4.99	4.93	9.81	8.03	42.31	1.0E+06	0.10
198.58	2.75	4.81	5.04	8.46	22.87	5.8E+05	0.20
176.69	2.02	4.80	9.98	7.58	14.99	3.1E+05	0.10
199.71	4.50	4.82	9.76	8.43	37.32	9.5E+05	0.10
199.81	4.91	4.85	8.55	8.32	40.93	1.0E+06	0.12
198.61	2.96	4.82	8.41	8.44	24.67	6.3E+05	0.12
168.55	2.67	4.84	10.00	7.10	18.93	3.4E+05	0.10
198.87	4.91	4.83	5.24	8.33	40.60	1.0E+06	0.19
199.32	4.32	4.84	8.90	8.34	35.95	9.1E+05	0.11
199.97	4.66	4.82	9.56	8.41	38.72	9.8E+05	0.10
195.25	2.75	4.81	9.94	8.34	22.46	5.5E+05	0.10
197.87	2.42	4.83	5.34	8.41	20.18	5.1E+05	0.19
199.21	3.89	4.82	9.15	8.42	32.33	8.2E+05	0.11
199.11	3.36	4.87	6.06	8.27	28.28	7.1E+05	0.16
183.75	2.03	4.80	9.57	7.89	15.64	3.4E+05	0.10
189.12	2.22	4.81	9.96	8.09	17.60	4.1E+05	0.10

It can be seen from the solution set that the diameter tends to the given maximum value, which means that the larger the diameter, the better the solution of the objective function. In the Pareto solution set, its length tends to the given minimum value, and the smaller the value, the better the performance. The optimal solution of the number of sections is mostly at the maximum value of the given, so that the extension ratio remains unchanged during the optimization process, so the maximum allowable number of sections can be given at the beginning of the design.

It can be seen from the Pareto solution set that the value of the objective function fluctuates, and there is a game among several objective function values. The parameter design should be selected according to the degree of importance and priority. The internal connections and changes between parameter values can be observe clearly in Figure 15.

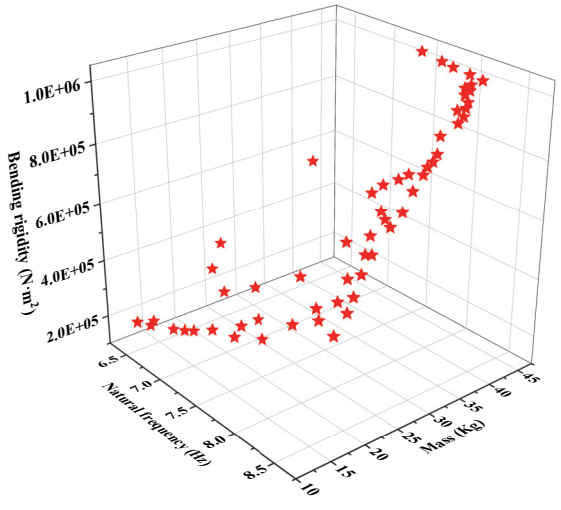

Figure 15 Pareto optimal solution of objective function

In addition to the game phenomenon between objective functions, there is also such a process between design parameters and target parameters, as shown in the Figure 16. The increase of the outer diameter will increase the natural frequency of the structure, which is roughly linear. In addition, it will also increase the bending rigidity of the structure and has a nonlinear relationship. The increase in the number of sections will inevitably lead to decrease in the extension ratio, making it possible to reduce the storage height. The increase in wall thickness will cause the bending rigidity increase, so the bending rigidity can be greatly improved if the outer diameter and wall thickness allow to change. 6 Deployment experiment with equivalent load

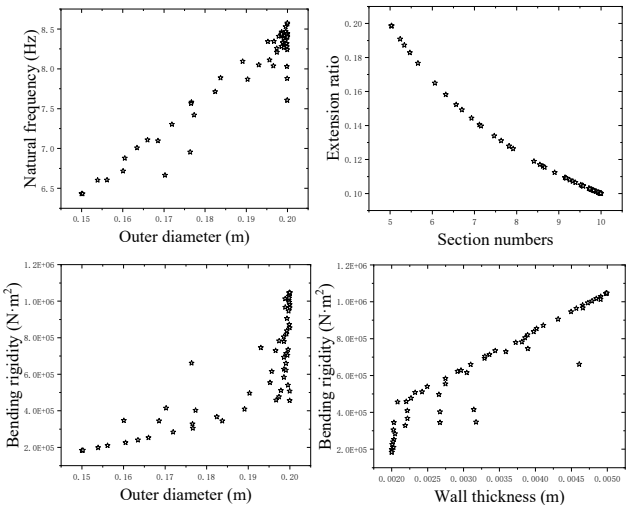

Figure 16 Game process between target parameters and design parameters

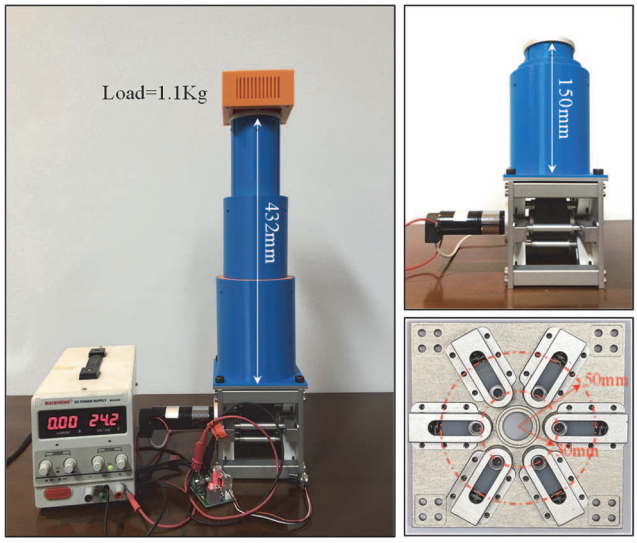

Figure 17 Prototype of TTM

In order to verify whether the extension arm can be extended under load, a proportional prototype was made based on the data selected from the Pareto solution set, as shown in Figure 17. The entire experimental process is completed in an ultra-clean laboratory.

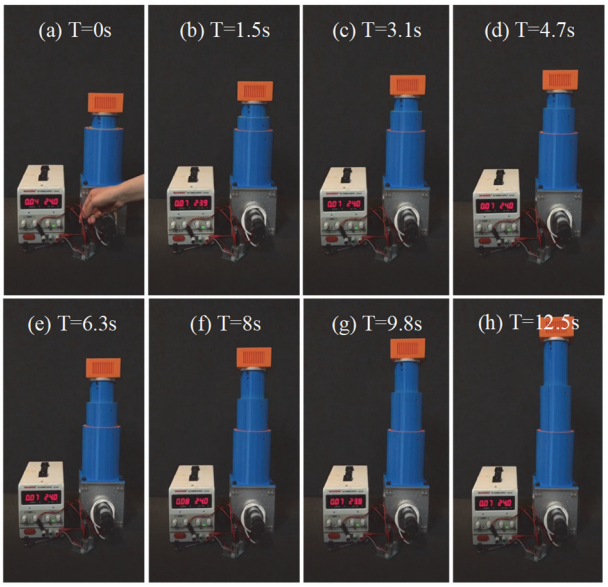

Figure 18 TTM working sequence with load

The drive motor model selects MD36NP51 planetary gear motor, the rated torque can reach 2.5N·m. The load and the TTM are connected by screws. The load of the solar sail is replaced by a cuboid of the same weight to complete the deployment experiment. The experiment process was repeated 10 times, and the deployment process and the repossession process were relatively stable. In addition, experiments were carried out with a load of 5 times the weight of the solar sail, and the deployment and repossession tasks were successfully completed, which verified the load capacity of the TTM. The whole experiment process takes 12.5s on average, and the time sequence is shown in Figure 18. In future experiments, the solar sail will be used for experiments to study whether the unfolding process will cause the vibration of the solar sail.

6 Conclusion

The main conclusions of this paper are as follows:

1) TTM driven by bistable carbon fiber is designed. It has the advantages of light weight, high precision, strong load capacity, and can be repeatedly deployed,

which is of great significance to meeting future space requirements.

2) The Euler-Bernoulli equivalent beam model and the segmented beam model are analyzed, and the natural frequency results are in good agreement.
3) The analysis results under different working conditions show that the performance is better when the two ends are fixed. The influence of multiple factors such as wall thickness on the vibration characteristics of the TTM is analyzed, which has guiding significance for the selection of design parameters.
4) The NASG-II multi-objective genetic algorithm is used to optimize the parameters of the natural frequency, mass, extension ratio, and bending rigidity of the TTM, and its Pareto solution set is obtained. It's very important for the parametric design of the TTM.
5) The processing prototype has been deployed under load, and the results show that the extension of the TTM and the repossession can be achieved smoothly.

The vibration generated during the working process is difficult to dissipate because of the special working environment of the TTM. Therefore, the vibration control will be carried out in future works. In addition, we will try to increase the strength and extension ratio of the TTM and reduce the weight.

7 Declaration

Funding

This work was supported by the National Key R&D Program of China (Grant No. 2018YFB1304600), the National Natural Science Foundation of China (Grant No. 51775541), the CAS Interdisciplinary Innovation Team (Grant No. JCTD-2018-11), the State Key Laboratory of Robotics Foundation (Grant No. Y91Z0303) and the Hundred-Talent Program (Chinese Academy of Sciences) (Grant No. Y8A3210304)

Authors' contributions

The author' contributions are as follows: Chenyang Ji was in charge of the whole trial; Chenyang Ji wrote the manuscript; Jinguo Liu, Chenchen Wu, Pengyuan Zhao and Keli Chen assisted with sampling and laboratory analyses; All authors read and approved the final manuscript.

Author Details

[1] State Key Laboratory of Robotics, Shenyang Institute of Automation, Chinese Academy of Science, Shenyang, 110016, China [2] School of Mechanical Engineering and Automation, Northeastern University, Shenyang 110819, China [3] Institutes for Robotics and Intelligent Manufacturing, Chinese Academy of Sciences, Shenyang 110169, China [4] University of Chinese Academy of Sciences, Beijing 100049, China

Authors' Information

Chen-Yang Ji, born in 1994, is currently a master candidate at *Northeastern University and State Key Laboratory of Robotics, Shenyang Institute of Automation, Chinese Academy of Science, China*. E-mail: jichenyang@sia.cn

Jinguo Liu, born in 1978, is currently a professor and a PhD candidate supervisor at *Shenyang Institute of Automation, Chinese Academy of Science, China*. E-mail: liujinguo@sia.cn

Chenchen Wu, born in 1990, is currently a associate professor at *Shenyang Institute of Automation, Chinese Academy of Science, China*. E-mail: wuchenchen@sia.cn

Pengyuan Zhao, born in 1994, is currently a PhD candidate at *State Key Laboratory of Robotics, Shenyang Institute of Automation, Chinese Academy of Science, China*. E-mail: zhaopengyuan@sia.cn

Keli Chen, born in 1991, is currently an engineer at *Shenyang Institute of Automation, Chinese Academy of Science, China*. E-mail: chenkeli@sia.cn

Competing interests

The authors declare no competing financial interests.

References

[1] Sosa E M, Thompson G J, Barbero E J. Experimental investigation of initial deployment of inflatable structures for sealing of rail tunnels. Tunnelling and Underground Space Technology, 2017, 69: 37-51.

[2] Mamalis A G, Manolakos D E, Ioannidis M B, et al. On the response of thin-walled CFRP composite tubular components subjected to static and dynamic axial compressive loading: experimental. Composite Structures, 2005, 69: 407-420.

[3] Houliara S, Karamanos S A. Buckling and post-buckling of long pressurized elastic thin-walled tubes under in-plane bending. International Journal of Non-Linear Mechanics, 2006, 41: 491-511.

[4] Yildiz K, Lesieutre G A. Sizing and prestress optimization of Class-2 tensegrity structures for space boom applications. Engineering with Computers, 2020: 1-14.

[5] Yang H, Guo H, Liu R, et al. Coiling and deploying dynamic optimization of a C-cross section thin-walled composite deployable boom. Structural and Multidiplinary Optimization, 2019, 61: 1731-1738.

[6] Bai J B, Shenoi R A, Xiong J J. Thermal analysis of thin-walled deployable composite boom in simulated space environment. Composite Structures, 2017, 173: 210-218.

[7] Bai J B, Chen D, Xiong J J, et al. Folding analysis for thin-walled deployable composite boom. Acta Astronautica, 2019, 159: 622-636.

[8] Firth J A, Pankow M R. Advanced Dual-Pull Mechanism for Deployable Spacecraft Booms. Journal of Spacecraft and Rockets,

2019, 56: 569-576.
[9] Ding X L, Xiao H, B, Yang Q L, et al. Design and analysis of a
[10] astrophysics missions. Acta Astronautica, 2020, 169: 124-137.
[11] Soykasap O. Deployment analysis of a self-deployable composite boom. Composite Structures, 2009, 89: 374-381.
[12] Walker S J I, Aglietti G S. A study of tape spring fold curvature for space deployable structures. Proceedings of the Institution of Mechanical Engineers -- Part G, 2007, 221: 313-325.
[13] Mallikarachchi H M Y C, Pellegrino S. Design of Ultrathin Composite Self-Deployable Booms. Journal of Spacecraft & Rockets, 2014, 51: 1811-1821.
[14] Liu Y, Du H, Liu L, et al. Shape memory polymers and their composites in aerospace applications: a review. Smart Materials & Structures, 2014, 23:23001-23022.
[15] Block J, Straubel M, Wiedemann M. Ultralight deployable booms for solar sails and other large gossamer structures in space. Acta Astronautica, 2011, 68: 984-992.
[16] Michael, A, Brown. A deployable mast for solar sails in the range of 100–1000 m. Advances in Space Research, 2011.
[17] Sickinger C, Herbeck L, Breitbach E. Structural engineering on deployable CFRP booms for a solar propelled sailcraft. Acta Astronautica, 2006, 58: 185-196.
[18] Zhao P Y, Liu J G, Wu C C. Survey on research and development of on-orbit active debris removal methods. Sci China Tech Sci, 2020, 63.
[19] Johnson, L, Young, R, Montgomery, et al. Status of solar sail cable-winding device driving large deployable mechanisms in

technology within nasa. Advances in Space Research, 2011, 48:1687-1694.
[20] Underwood C, Viquerat A, Schenk M, et al. InflateSail de-orbit flight demonstration results and follow-on drag-sail applications. Acta astronautica, 2019, 162:3 44-358.
[21] Juan M Fernandez, Lourens Visagie, Mark Schenk, et al. Design and development of a gossamer sail system for deorbiting in low earth orbit. Acta Astronautica, 2014, 103: 204-225.
[22] Wei J Z, Ma R Q, Liu Y F, et al. Modal analysis and identification of deployable membrane structures. Acta Astronautica, 2018, 152: 811-822.
[23] Schenk M, Viquerat A D, Seffen K A, et al. Review of inflatable booms for deployable space structures: packing and rigidization. Journal of Spacecraft and Rockets, 2014, 51: 762-778.
[24] Sosa E M, Wong C S, Adumitroaie A, et al. Finite element simulation of deployment of large-scale confined inflatable structures. Thin Walled Structures, 2016, 104: 152-167.
[25] Katsumata N, Natori M C, Yamakawa H. Analysis of dynamic behaviour of inflatable booms in zigzag and modified zigzag folding patterns Acta Astronautica, 2014, 93: 45-54.
[26] Deb K, Pratap A, Agarwal s, et al. A Fast and elitist multiobjective genetic algorithm: NSGA-II, IEEE Transactions on Evolutionary Computation, 2002, 6: 182-197.

Figures

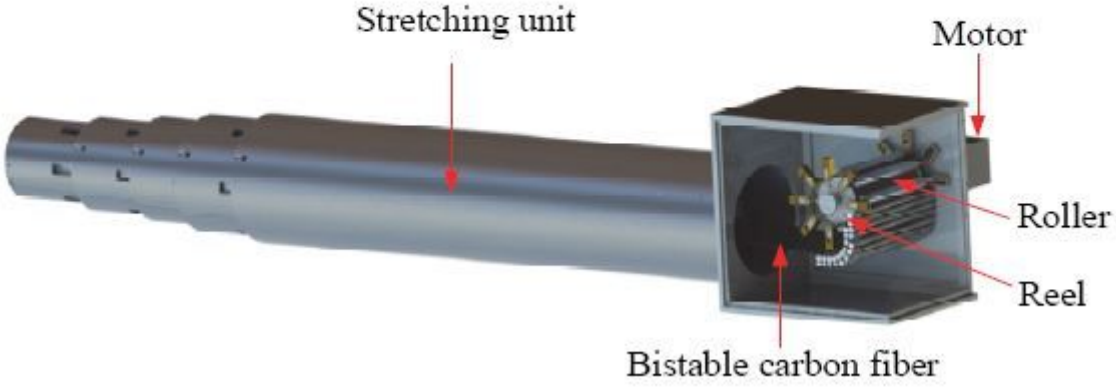

Figure 1

The main structure of each part of the TTM

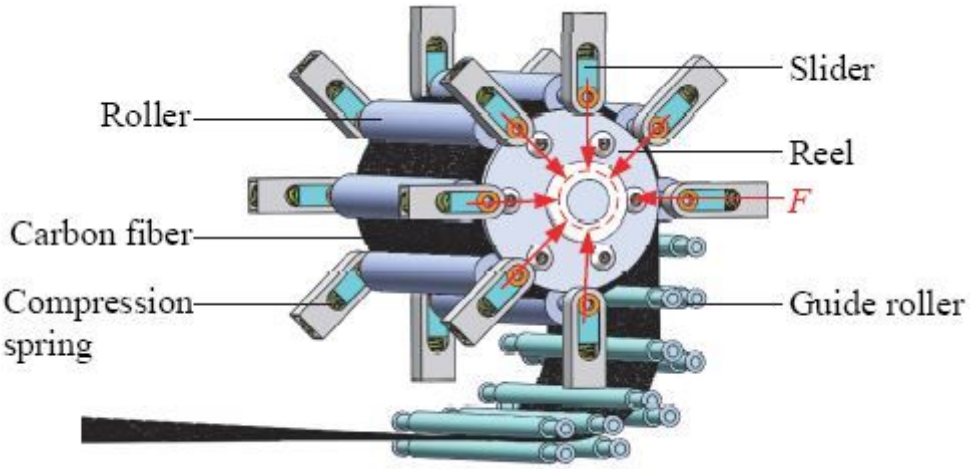

Figure 2

Drive and anti-blossoming structure

Figure 3

Solar Sail Load at the tip of TTM

Figure 4

Work flow of TTM and solar sail

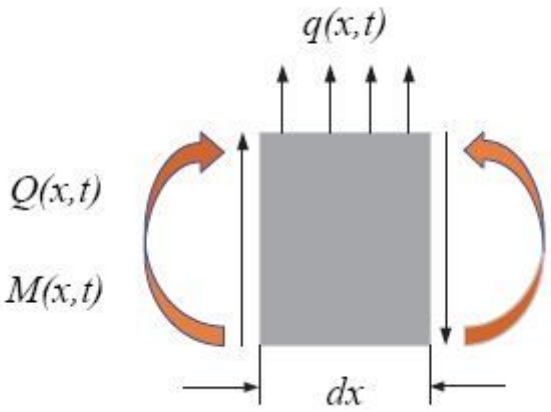

Figure 5

Equivalent beam micro-element segment model

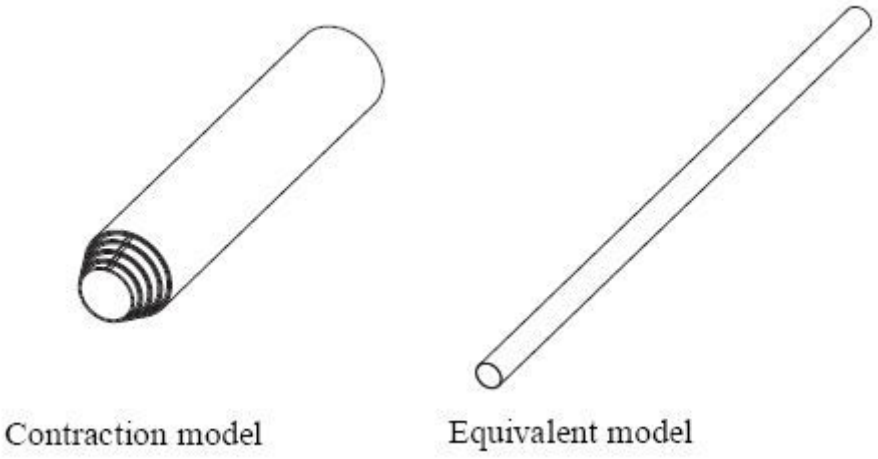

Figure 6

Model of TTM contraction and extension state

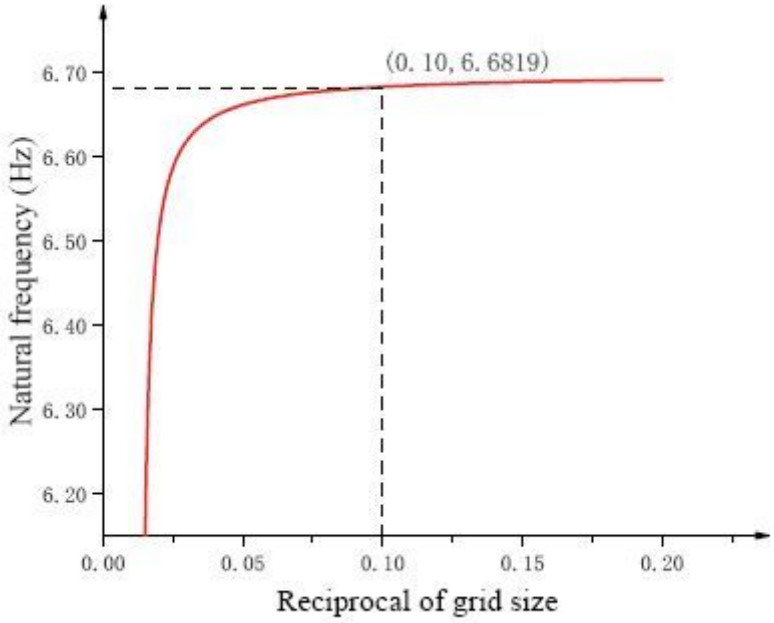

Figure 7

Mesh size convergence analysis

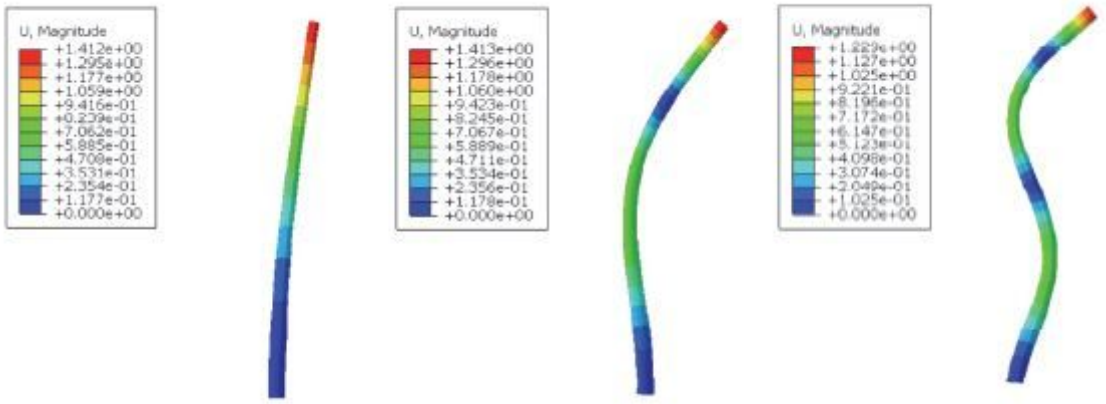

Figure 8

Modal shape of the segmented model of the TTM

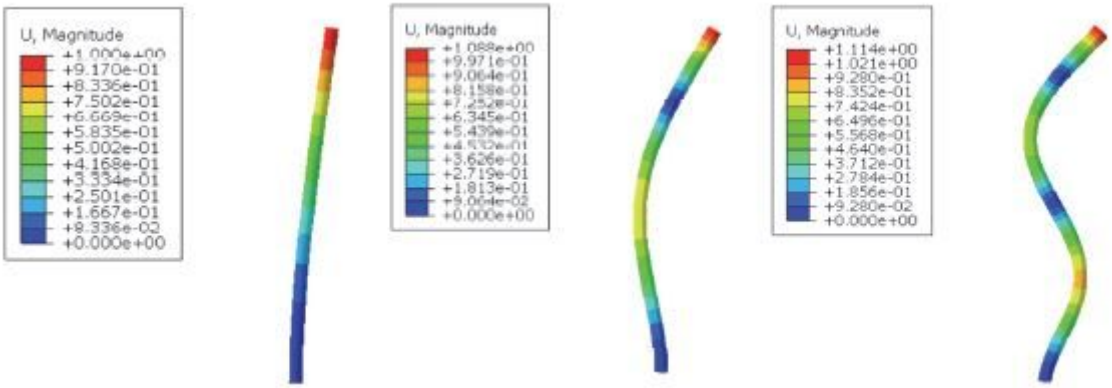

Figure 9

Modal shape of the equivalent model of the TTM

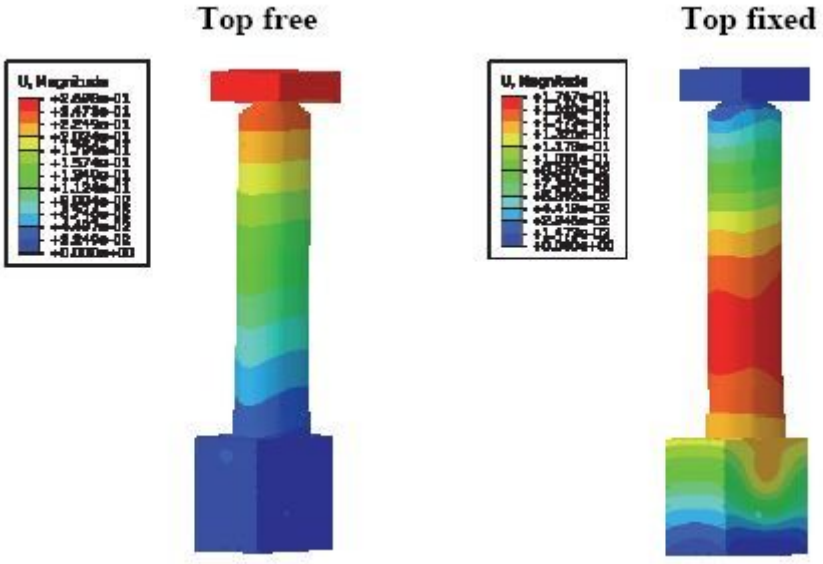

Figure 10

Displacement cloud diagram under two conditions

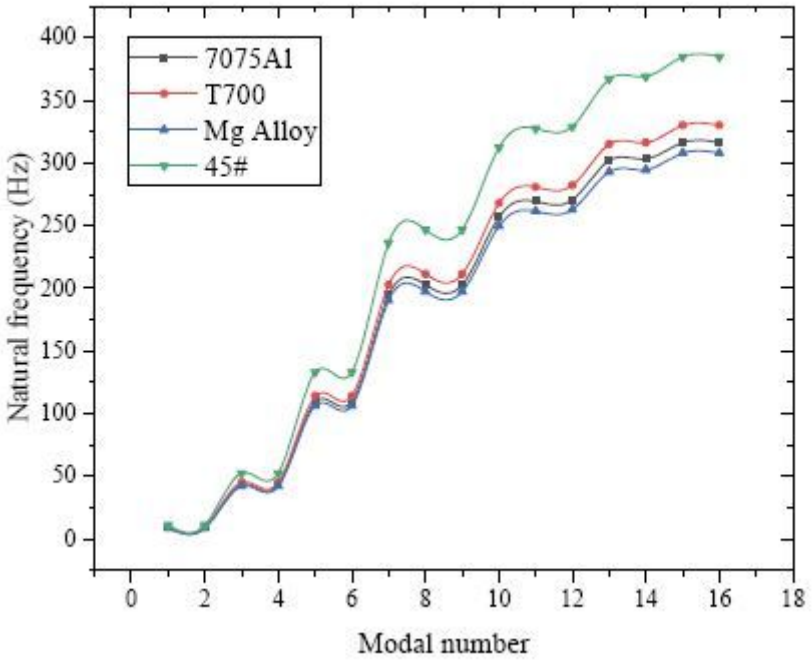

Figure 11

The influence of material on vibration characteristics

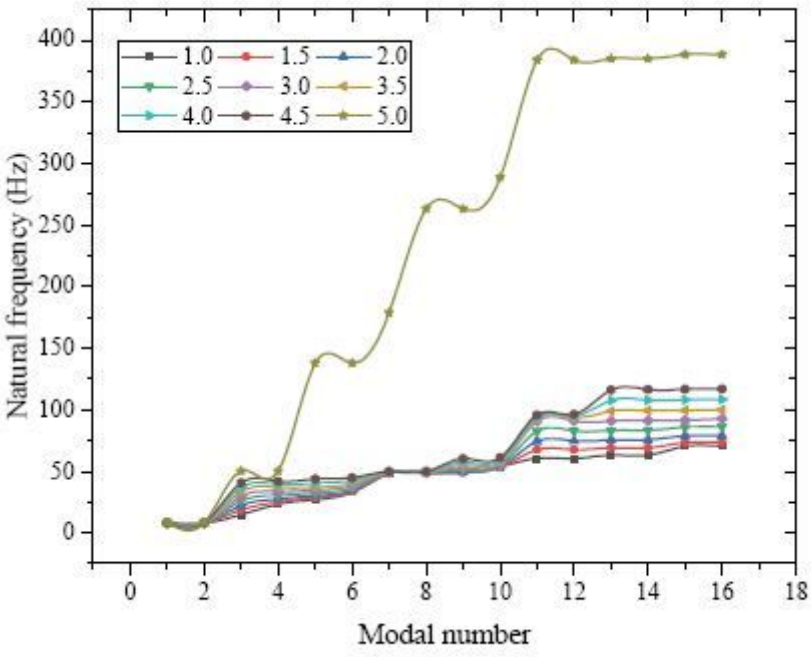

Figure 12

The influence of wall thickness on vibration characteristics

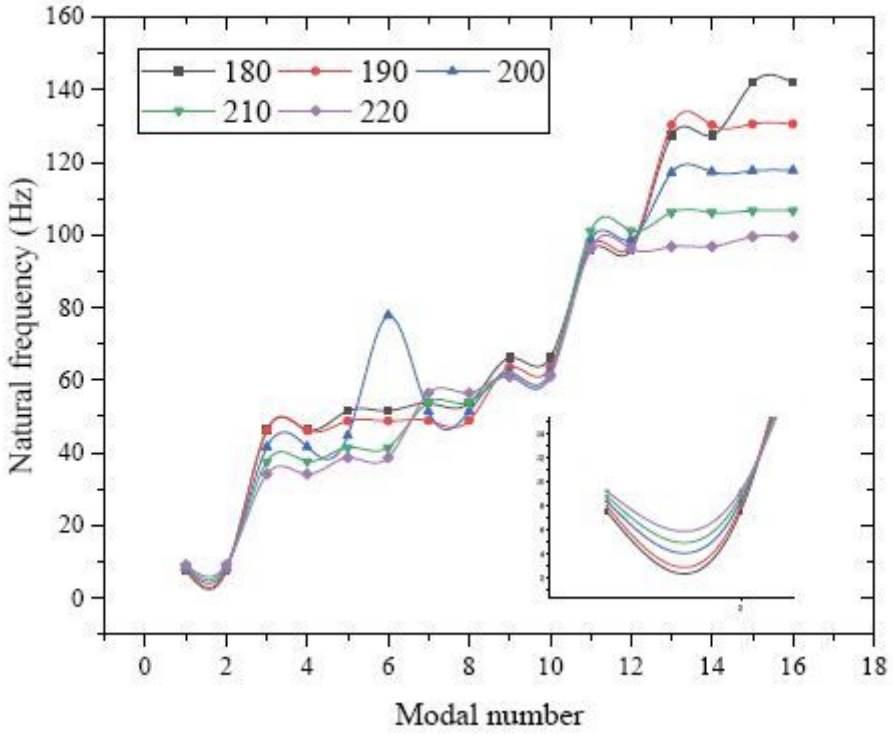

Figure 13

The influence of diameter on vibration characteristics

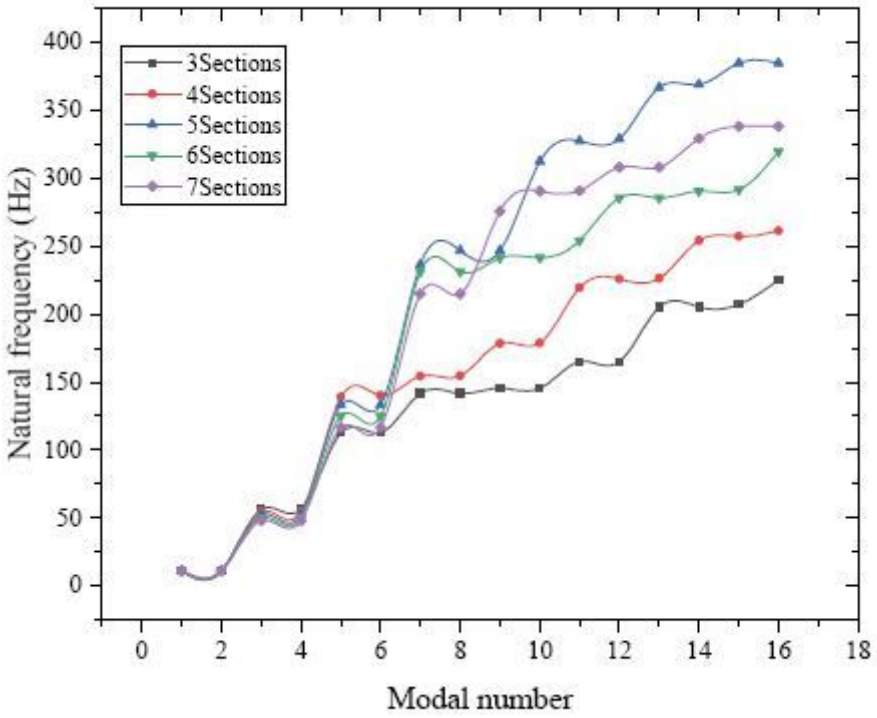

Figure 14

The influence of number of sections on vibration characteristics

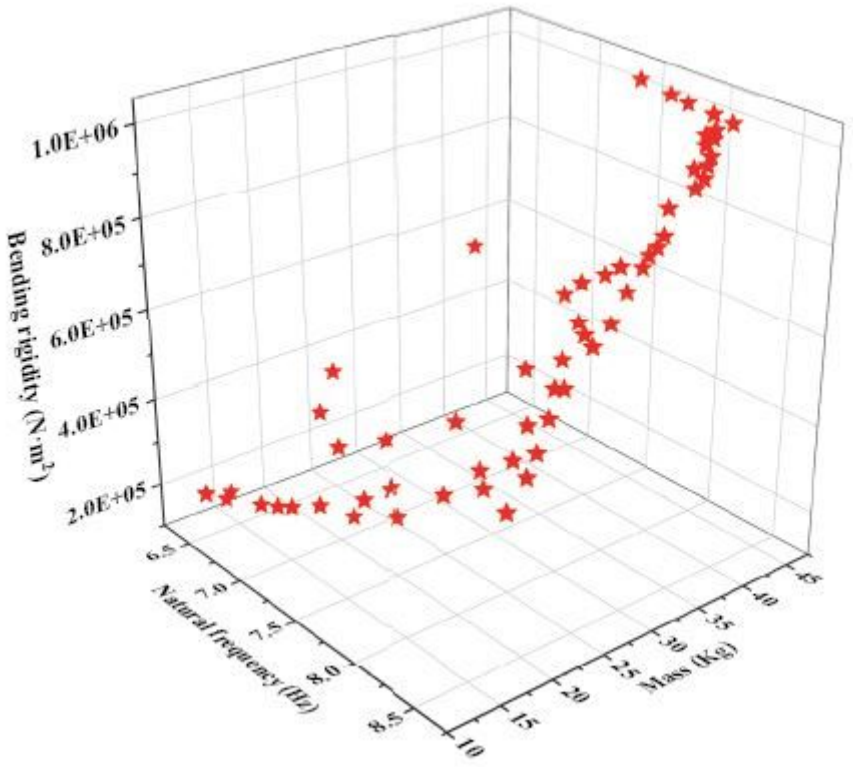

Figure 15

Pareto optimal solution of objective function

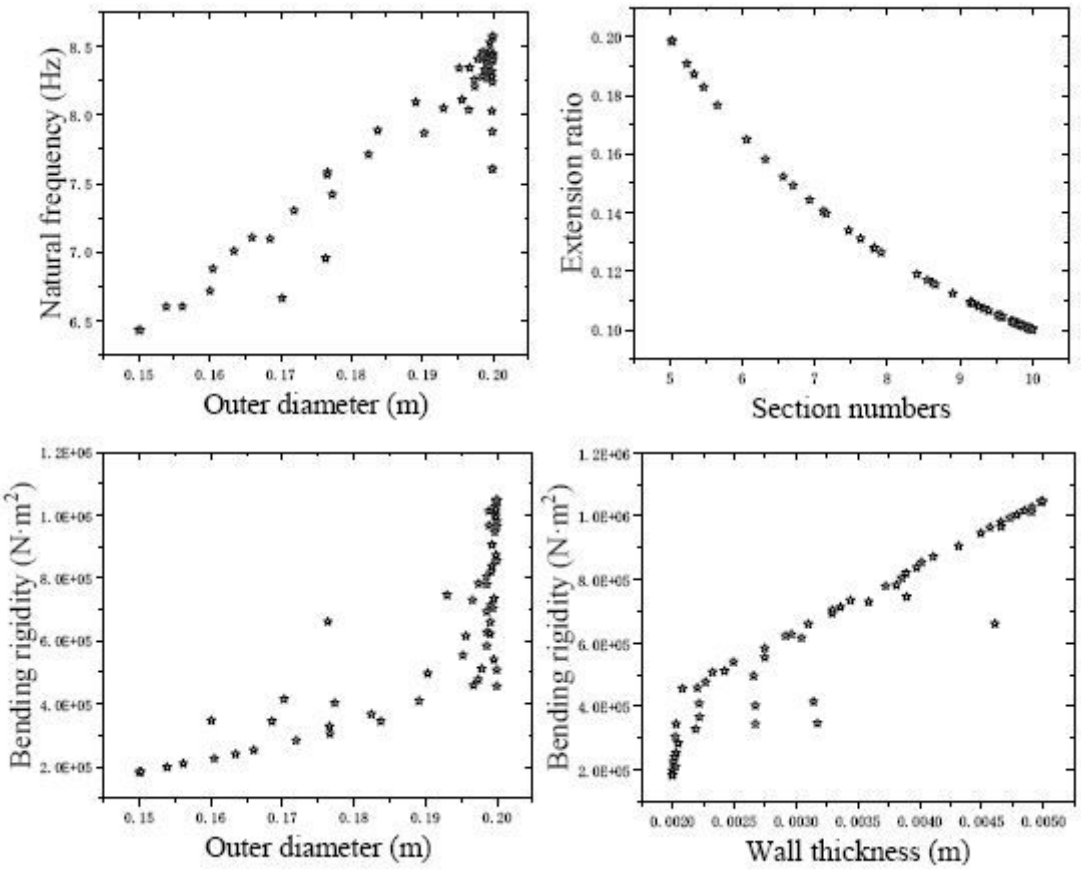

Figure 16

Game process between target parameters and design parameters

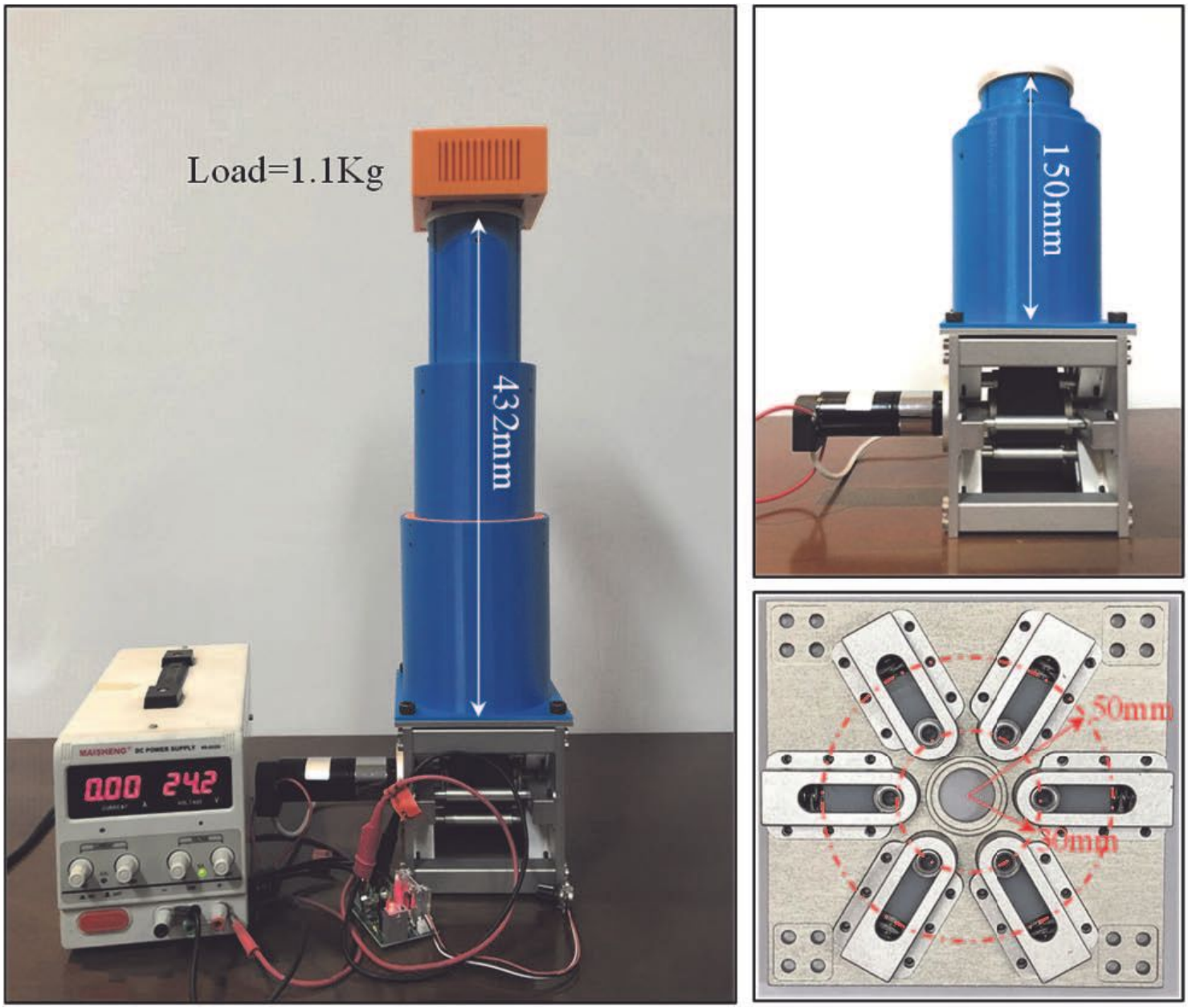

Figure 17

Prototype of TTM

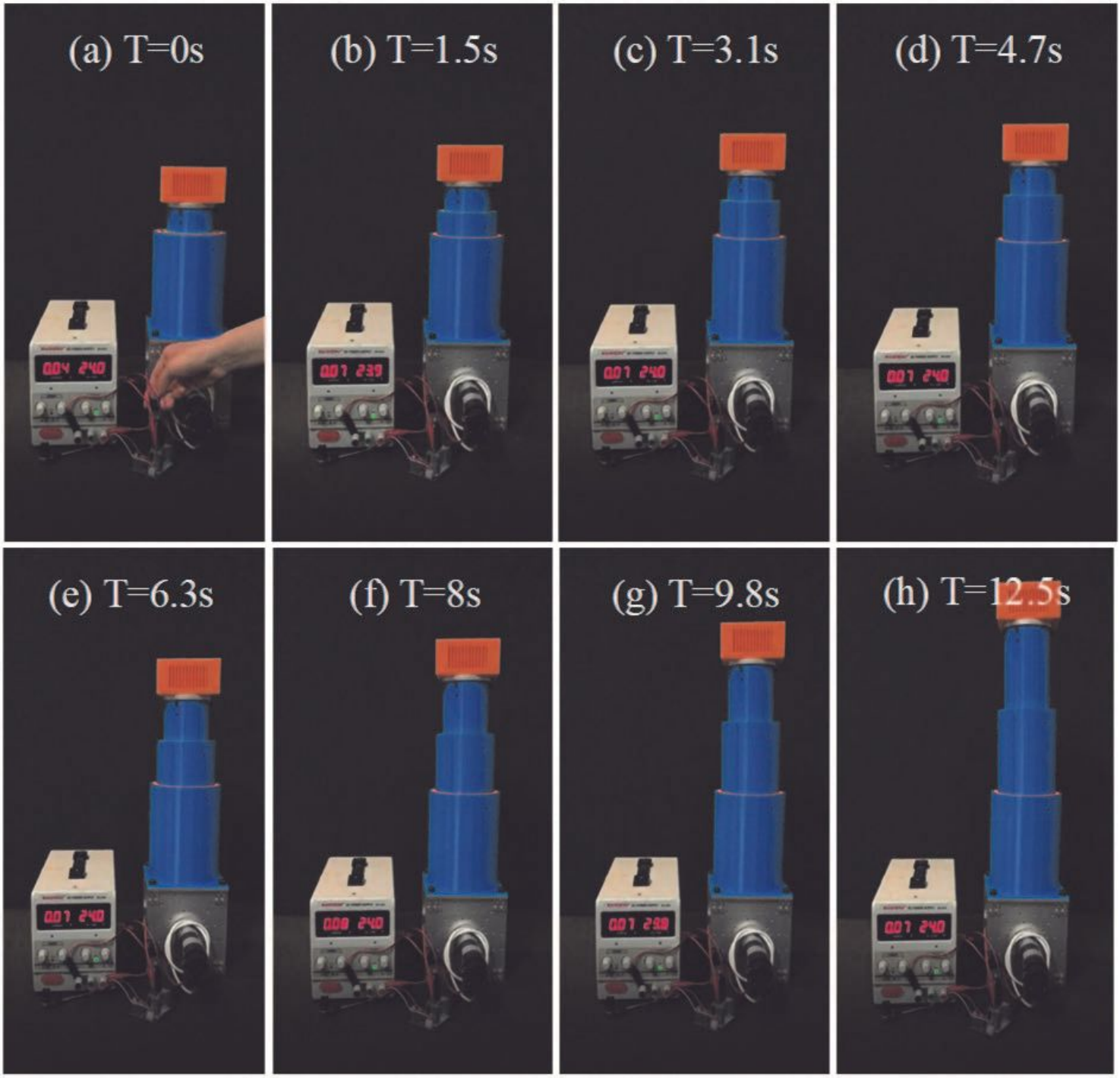

Figure 18

TTM working sequence with load